



Article

# Protein Profiling of WERI-RB1 and Etoposide-Resistant WERI-ETOR Reveals New Insights into Topoisomerase Inhibitor Resistance in Retinoblastoma

Vinodh Kakkassery <sup>1,\*</sup>,<sup>†</sup> Timo Gemoll <sup>2,†</sup>, Miriam M. Kraemer <sup>3</sup>, Thorben Sauer <sup>2</sup>, Aysegül Tura <sup>1</sup>, Mahdy Ranjbar <sup>1</sup>, Salvatore Grisanti <sup>1</sup>, Stephanie C. Joachim <sup>4</sup>, Stefan Mergler <sup>5</sup> and Jacqueline Reinhard <sup>3,\*</sup>

- <sup>1</sup> Department of Ophthalmology, University of Luebeck, Ratzeburger Allee 160, 23538 Luebeck, Germany; ayseguel.tura@uksh.de (A.T.); mahdy.ranjbar@uksh.de (M.R.); salvatore.grisanti@uksh.de (S.G.)
  - <sup>2</sup> Section for Translational Surgical Oncology and Biobanking, Department of Surgery, University of Luebeck and University Hospital Clinic Schleswig-Holstein, Ratzeburger Allee 160, 23538 Luebeck, Germany; timo.gemoll@uni-luebeck.de (T.G.); thorben.sauer@student.uni-luebeck.de (T.S.)
  - <sup>3</sup> Department of Cell Morphology and Molecular Neurobiology, Faculty of Biology and Biotechnology, Ruhr-University Bochum, Universitaetsstraße 150, 44780 Bochum, Germany; m.kraemer@mmk2.de
  - <sup>4</sup> Experimental Eye Research Institute, University Eye Hospital, Ruhr-University Bochum, In der Schornau 23-25, 44892 Bochum, Germany; stephanie.joachim@rub.de
  - <sup>5</sup> Department of Ophthalmology, Charité-Universitaetsmedizin Berlin, Corporate Member of Freie Universitaet Berlin, Humboldt-Universitaet zu Berlin, Augustenberger Platz 1, 13353 Berlin, Germany; stefan.mergler@charite.de
- \* Correspondence: vinodh.kakkassery@gmail.com (V.K.); jacqueline.reinhard@rub.de (J.R.); Tel.: +49-451-500-43911 (V.K.); +49-234-32-24-314 (J.R.)
- † These authors contributed equally to this work.



**Citation:** Kakkassery, V.; Gemoll, T.; Kraemer, M.M.; Sauer, T.; Tura, A.; Ranjbar, M.; Grisanti, S.; Joachim, S.C.; Mergler, S.; Reinhard, J. Protein Profiling of WERI-RB1 and Etoposide-Resistant WERI-ETOR Reveals New Insights into Topoisomerase Inhibitor Resistance in Retinoblastoma. *Int. J. Mol. Sci.* **2022**, *23*, 4058. <https://doi.org/10.3390/ijms23074058>

Academic Editor: Toshihide Kurihara

Received: 20 February 2022

Accepted: 2 April 2022

Published: 6 April 2022

**Publisher's Note:** MDPI stays neutral with regard to jurisdictional claims in published maps and institutional affiliations.



**Copyright:** © 2022 by the authors. Licensee MDPI, Basel, Switzerland. This article is an open access article distributed under the terms and conditions of the Creative Commons Attribution (CC BY) license (<https://creativecommons.org/licenses/by/4.0/>).

**Abstract:** Chemotherapy resistance is one of the reasons for eye loss in patients with retinoblastoma (RB). RB chemotherapy resistance has been studied in different cell culture models, such as WERI-RB1. In addition, chemotherapy-resistant RB subclones, such as the etoposide-resistant WERI-ETOR cell line have been established to improve the understanding of chemotherapy resistance in RB. The objective of this study was to characterize cell line models of an etoposide-sensitive WERI-RB1 and its etoposide-resistant subclone, WERI-ETOR, by proteomic analysis. Subsequently, quantitative proteomics data served for correlation analysis with known drug perturbation profiles. Methodically, WERI-RB1 and WERI-ETOR were cultured, and prepared for quantitative mass spectrometry (MS). This was carried out in a data-independent acquisition (DIA) mode. The raw SWATH (sequential window acquisition of all theoretical mass spectra) files were processed using neural networks in a library-free mode along with machine-learning algorithms. Pathway-enrichment analysis was performed using the REACTOME-pathway resource, and correlated to the molecular signature database (MSigDB) hallmark gene set collections for functional annotation. Furthermore, a drug-connectivity analysis using the L1000 database was carried out to associate the mechanism of action (MOA) for different anticancer reagents to WERI-RB1/WERI-ETOR signatures. A total of 4756 proteins were identified across all samples, showing a distinct clustering between the groups. Of these proteins, 64 were significantly altered ( $q < 0.05$  &  $\log_2FC > 2$ , 22 higher in WERI-ETOR). Pathway analysis revealed the “retinoid metabolism and transport” pathway as an enriched metabolic pathway in WERI-ETOR cells, while the “sphingolipid de novo biosynthesis” pathway was identified in the WERI-RB1 cell line. In addition, this study revealed similar protein signatures of topoisomerase inhibitors in WERI-ETOR cells as well as ATPase inhibitors, acetylcholine receptor antagonists, and vascular endothelial growth factor receptor (VEGFR) inhibitors in the WERI-RB1 cell line. In this study, WERI-RB1 and WERI-ETOR were analyzed as a cell line model for chemotherapy resistance in RB using data-independent MS. Analysis of the global proteome identified activation of “sphingolipid de novo biosynthesis” in WERI-RB1, and revealed future potential treatment options for etoposide resistance in RB.

**Keywords:** chemotherapy resistance; mass spectrometry; retinoblastoma; WERI-ETOR; WERI-RB1

## 1. Introduction

To date, retinoblastoma (RB) has an incidence of 1/15,000 to 1/20,000 live births, and around 9000 new cases are diagnosed worldwide every year [1–4]. This makes it the most common malignant pediatric ocular tumor globally. Due to an improvement in therapeutic strategies in recent years, the survival rate in western countries is almost 99%, while death rates in Africa and Asia are still high [5–7]. Unfortunately, some affected eyes still need to be removed due to chemotherapy failure, which is also due to chemotherapy resistance [8].

Chemotherapy-resistance mechanisms in RB are unclear so far. To further investigate the mechanisms in RB, the WERI-RB1 cell line (Leibniz Institute–German Collection of Microorganisms and Cell Cultures, DSMZ No. ACC90) has been established by spontaneous outgrowth of an enucleated RB eye, as published by McFall et al. [9,10]. Among others, Busch et al. characterized the growth behavior of the WERI-RB1 cell line under cell-culture conditions [11]. To identify the mechanisms of chemotherapy resistance, the etoposide-resistant subclone WERI-ETOR was established by harvesting surviving cells after incubation with increasing etoposide doses from WERI-RB1, as described by Stephan et al. [12]. Previous studies also examined the parental WERI-RB1 and the etoposide-resistant subclone WERI-ETOR on the molecular level [13–18]. Furthermore, Busch et al. demonstrated a higher proliferation rate in WERI-ETOR as well as increased tumor formation and tumor size in an *in vivo* chick chorioallantoic-membrane assay [17]. Mergler et al. and Oronowicz et al. showed alterations in thermosensitive transient receptor potential channels in WERI-ETOR cells [13,16]. A publication by Kakkassery et al. proved an upregulation of sphingosine-1-phosphate in the WERI-ETOR cell line as a potential resistance mechanism in RB [14]. Recently, Reinhard et al. reported on changes of the extracellular matrix (ECM) in WERI-ETOR compared to WERI-RB1 cells [15].

Interestingly, the nature of the global proteome in RB remains unclear. While genotype–phenotype relationships are complex, proteins are generally known to be the effectors. However, molecular signatures associated with a phenotype of interest could also occur on a different level, e.g., as expression signatures and methylation signatures [19–22]. As such, proteins are suited to determine the signature of a physiological phenotype as well as the point of intervention for drug and health treatments. Hereby, LC-ESI-MS/MS in a data-independent (DIA/SWATH) mode plays a decisive role. DIA/SWATH uses variable mass windows to enable the complete measurement of all detectable proteins in a sample. This allows the identification and quantification of thousands of proteins in just one measurement. Compared to alternative relative quantification techniques, such as iTRAQ, label-free SWATH offers higher sensitivity, reliability, and robustness. Furthermore, sample preparation for labeled proteomics is more complex as it requires, e.g., the covalent binding of isobaric labels to the peptide analytes [23]. Therefore, the specific aim of this study was to characterize the differences between the cell lines WERI-RB1 and WERI-ETOR on the proteomic level. The data for this investigation was collected by quantitative mass spectrometry (MS) in DIA mode in combination with machine-learning algorithms for mass spectrometric and statistical evaluation. The generated quantitative proteome data was used to gain further insight into the functional annotation, including intracellular-signaling pathways that differ between WERI-RB1 and WERI-ETOR. Furthermore, a drug-connectivity analysis using the L1000 database was used to correlate the mechanism of action (MOA) for different anticancer reagents to WERI-RB1/WERI-ETOR signatures.

## 2. Results

### 2.1. Protein-Expression Profiles of WERI-RB1 and WERI-ETOR Cell Lines

We performed quantitative MS using a DIA mode to detect proteins differentially expressed in WERI-RB1 and WERI-ETOR cell lines. Using a neuronal network-based identification workflow (DIA-NN, [24]), 4756 protein groups were identified. All entries with more than 70% missing values (MV) were removed, resulting in 2.2% MVs. The remaining MVs were imputed via replacement by random draws from a normal distribution. A table containing all protein quantification values is included in Supplemental Table S1. MS data

have been deposited to the ProteomeXchange Consortium via the PRIDE partner repository with the dataset identifier PXD030924.

Phenotypic differences between both cell cultures were compared in a t-distributed stochastic neighbor embedding (tSNE) applying protein-expression data. A tSNE plot showed a clear differentiation of the analyzed groups (Figure 1).

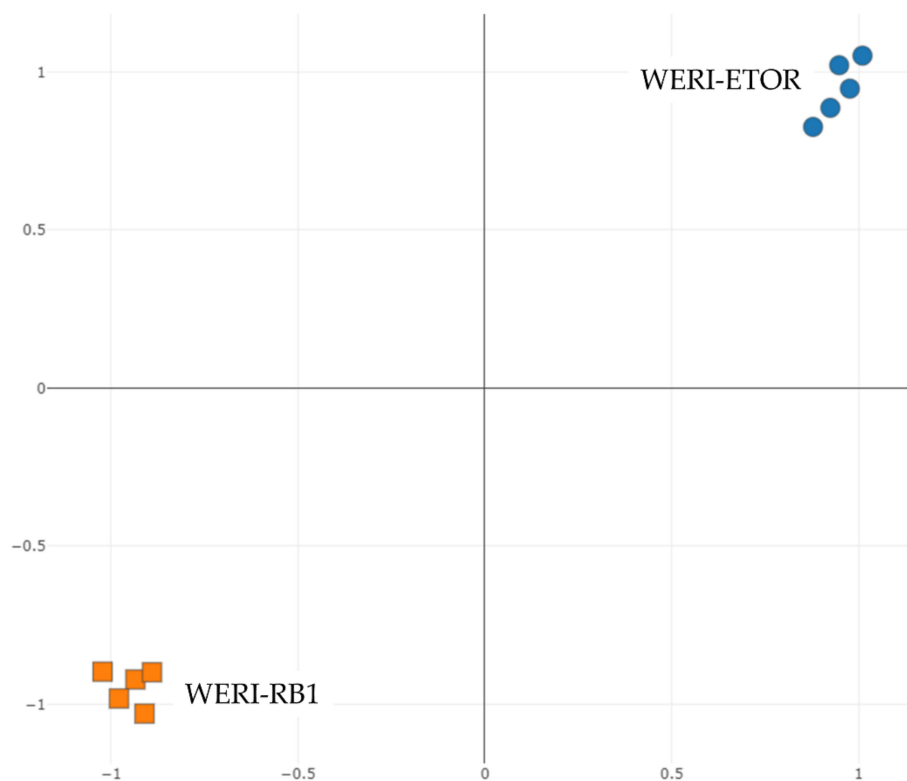


**Figure 1.** Unsupervised tSNE plot of WERI-RB1 (orange) and WERI-ETOR (blue) cell-line samples. The plot visualizes the close relationship with cell lines and the distinct clustering between sample groups ( $n = 5/\text{group}$ ).

A total of 64 differentially expressed proteins ( $q < 0.05$  &  $\log_2\text{FC} | > 2 |$ ) were found between the two groups. Of these proteins, 22 (34%) showed a higher concentration, while 42 (66%) had a lower concentration in the WERI-ETOR cell line (Figure 2). The protein with the highest differential expression in WERI-ETOR was dehydrogenase/reductase 2 (DHRS2;  $q$ -value: 0.0000305 and  $\log_2\text{FC}$ : 4.06), whereas H1.5 linker histone, cluster member (H1-5) showed the highest differential expression in WERI-RB1 ( $q$ -value: 0.00000285 and  $\log_2\text{FC}$ :  $-7.81$ ). A list of all differentially expressed proteins, including their corresponding  $\log_2\text{FC}$  and  $q$  values, is shown in Supplemental Table S2.

For validation of differential-expressed proteins, a feature importance calculation based on machine-learning algorithms (LASSO, elastic nets, random forest, extreme gradient boosting) selected the best possible proteins ( $n = 40$ ) to predict group association (Table 1). What stands out in the table is that all top important features also showed statistical significance. Additionally, the most important proteins are displayed using a heatmap clustering (Figure 3).

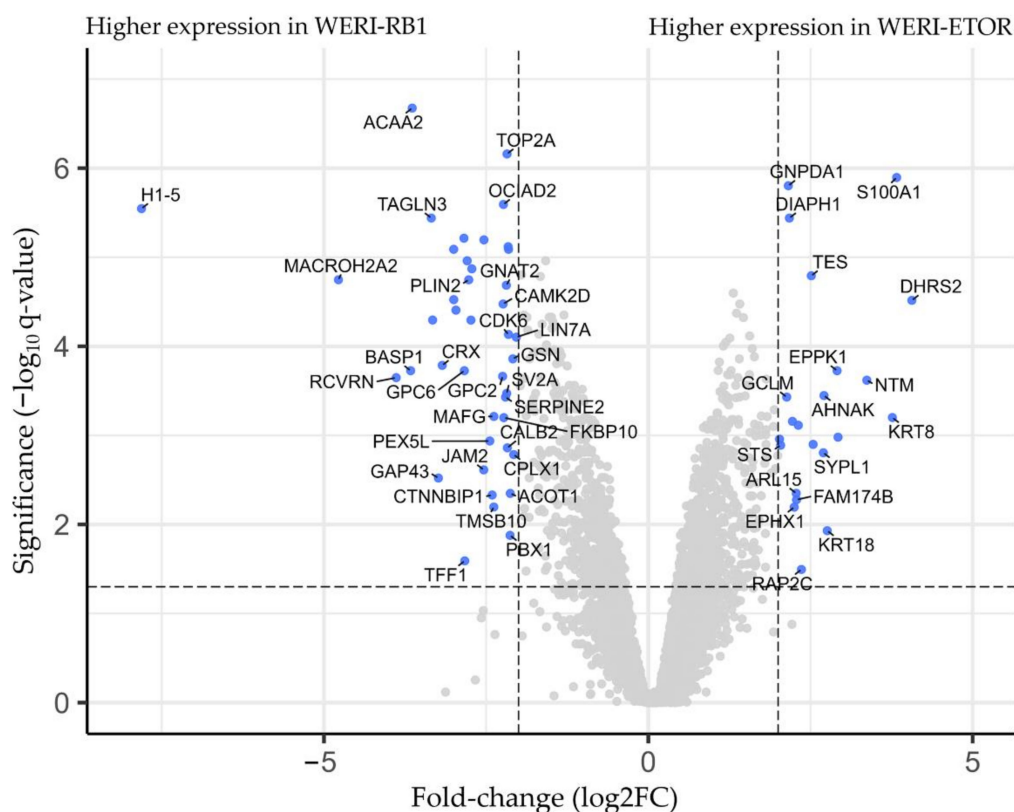


**Figure 2.** Volcano plot visualizing fold-change (x-axis) and statistical significance (y-axis). Proteins with a higher concentration in the WERI-ETOR cell line are presented on the right side. Proteins with a lower concentration in the WERI-ETOR cell line are displayed on the left side. All blue-marked proteins demonstrated a logarithmic fold-change (log2FC) of  $|>2|$  and a q-value  $< 0.05$ .

**Table 1.** Top 40 differentially expressed proteins between WERI-RB1 and WERI-ETOR cell lines detected by machine-learning algorithms (LASSO, elastic nets, random forests, extreme gradient boosting). Proteins are sorted according to their fold-change. Log fold-change  $> 0$  represents a higher expression of the protein in the WERI-ETOR group. Significance was calculated using four commonly accepted methods in the literature (Welch *t*-test, limma, edgeR, DESeq2) and merged (meta.q-value).

Gene Symbol	Full Protein Name	Chromosome	Meta.q-Value	Log Fold-Change [WERI-ETOR/WERI-RB1]
DHRS2	Dehydrogenase/reductase SDR family member 2	14	$3.051 \times 10^{-5}$	4.062
S100A1	Protein S100-A1	1	$1.275 \times 10^{-6}$	3.828
KRT8	Keratin 8	12	$6.307 \times 10^{-4}$	3.762
NTM	NAC domain-containing protein 69	11	$2.402 \times 10^{-4}$	3.368
EPPK1	Epiplakin	8	$1.879 \times 10^{-4}$	2.910
AHNAK	AHNAK nucleoprotein	11	$3.570 \times 10^{-4}$	2.708
SEPTIN6	Septin 6	X	$1.262 \times 10^{-4}$	2.540
TES	Testin	7	$1.615 \times 10^{-5}$	2.513
DIAPH1	Protein diaphanous homolog 1	5	$3.634 \times 10^{-6}$	2.174
GNPDA1	Glucosamine-6-phosphate isomerase 1	5	$1.576 \times 10^{-6}$	2.158

Table 1. Cont.

Gene Symbol	Full Protein Name	Chromosome	Meta.q-Value	Log Fold-Change [WERI-ETOR/WERI-RB1]
CRLF3	Cytokine receptor like factor 3	17	$5.155 \times 10^{-4}$	1.942
MEX3A	RNA-binding protein MEX3A	1	$4.712 \times 10^{-5}$	-1.871
CDH2	Cadherin-2	18	$1.581 \times 10^{-5}$	-1.955
TOP2B	DNA topoisomerase 2-beta	3	$8.151 \times 10^{-6}$	-2.155
CDK6	Cyclin-dependent kinase 6	7	$7.362 \times 10^{-5}$	-2.156
ATP2B1	Plasma membrane calcium-transporting ATPase 1	12	$7.630 \times 10^{-6}$	-2.160
TOP2A	DNA topoisomerase 2-alpha	17	$6.932 \times 10^{-7}$	-2.178
GNAT2	Guanine nucleotide-binding protein G(t) subunit alpha-2	1	$2.064 \times 10^{-5}$	-2.189
SERPINE2	Serpin family E member 2	2	$3.716 \times 10^{-4}$	-2.201
OCIAD2	OCIA domain-containing protein 2	4	$2.556 \times 10^{-6}$	-2.234
CAMK2D	Calcium-dependent protein kinase II	4	$3.350 \times 10^{-5}$	-2.238
CTNBP1	Catenin-beta-interacting protein 1	1	$4.668 \times 10^{-3}$	-2.408
LMOD1	Leiomodin-1	1	$6.385 \times 10^{-6}$	-2.534
ACBD7	Acyl-CoA-binding domain-containing protein 7	10	$1.349 \times 10^{-5}$	-2.720
GDAP1L1	Ganglioside-induced differentiation-associated protein 1-like 1	20	$5.081 \times 10^{-5}$	-2.734
PLIN2	Perilipin-2	9	$1.793 \times 10^{-5}$	-2.769
DPYSL3	Dihydropyrimidinase like 3	5	$1.096 \times 10^{-5}$	-2.792
AMPH	D-alanyl-D-alanine-carboxypeptidase/endorpeptidase AmpH	7	$6.121 \times 10^{-6}$	-2.842
MAP2	Microtubule-associated protein 2	2	$3.928 \times 10^{-5}$	-2.966
ATP1B1	Sodium/potassium-transporting ATPase subunit beta-1	1	$2.994 \times 10^{-5}$	-3.000
GNGT2	Guanine nucleotide-binding protein subunit gamma-T2	17	$8.151 \times 10^{-6}$	-3.000
CRX	Cone-rod homeobox protein	19	$1.636 \times 10^{-4}$	-3.177
GAP43	Neuromodulin	3	$3.011 \times 10^{-3}$	-3.236
SH3BGRL	SH3 domain-binding glutamic acid-rich-like protein 3	X	$5.071 \times 10^{-5}$	-3.325
TAGLN3	Transgelin-3	3	$3.634 \times 10^{-6}$	-3.346
ACAA2	3-ketoacyl-CoA thiolase	18	$2.119 \times 10^{-7}$	-3.640
BASP1	Brain-acid-soluble protein 1	5	$1.879 \times 10^{-4}$	-3.664
RCVRN	Recoverin	17	$2.248 \times 10^{-4}$	-3.886
MACROH2A2	Core histone macro-H2A.2	10	$1.791 \times 10^{-5}$	-4.777
H1-5	Histone H1.5	6	$2.846 \times 10^{-6}$	-7.812

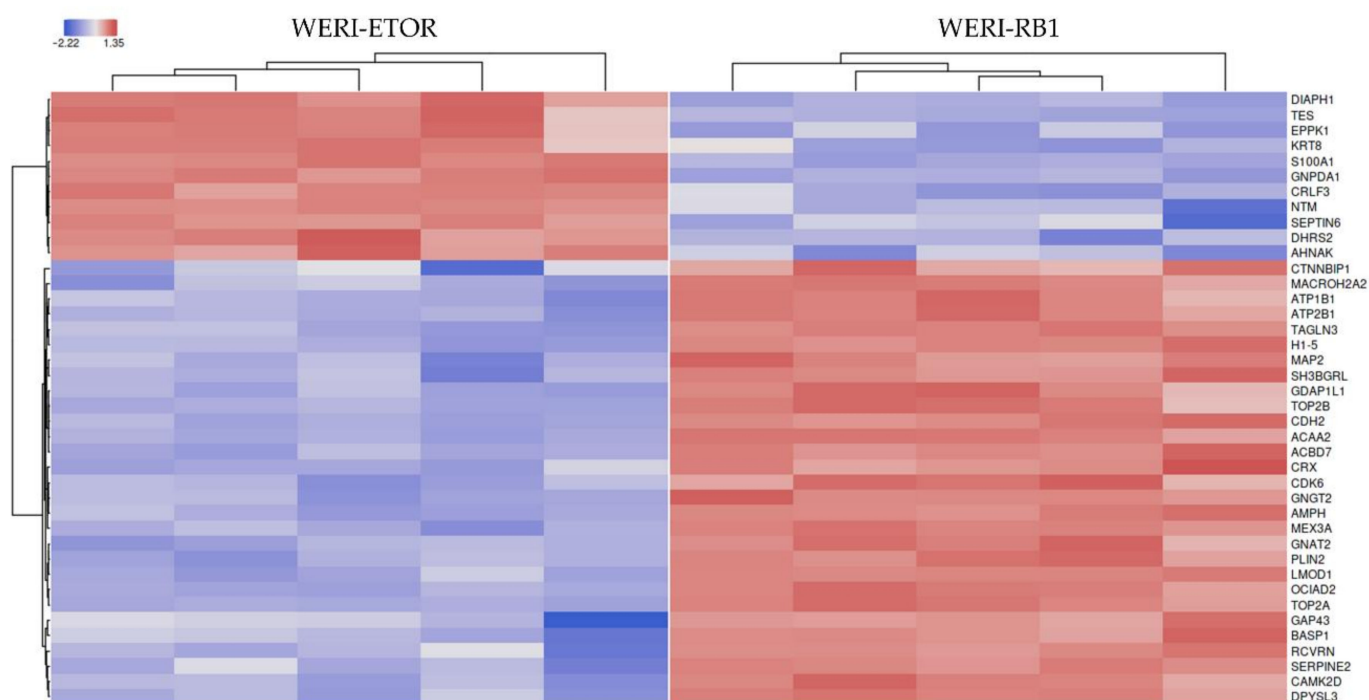


**Figure 3.** Heatmap of the top 40 selected features according to a cumulative ranking by the applied algorithms (LASSO, elastic nets, random forest, extreme gradient boosting). Red colors show high protein expression, and blue colors show low protein expression.

## 2.2. Enrichment-Pathway Analysis of WERI-RB1 and WERI-ETOR Protein Signatures

For a deeper insight into the different proteomes of the WERI-RB1 and WERI-ETOR cell lines, all proteins were uploaded to the REACTOME database. The REACTOME-pathway-enrichment algorithm was able to match 3934 out of 4756 (83%) proteins, which were associated with 2026 available pathways (submission date: May 2021). Among others, one of the most enriched metabolic pathways for the WERI-ETOR was “retinoid metabolism and transport” ( $p = 0.0029$ ), while “sphingolipid de novo biosynthesis” ( $p = 0.033$ ) was activated in WERI-RB1. Eleven identified proteins were represented in the network of “retinoid metabolism and transport”: retinol dehydrogenase 11 (RDH11), agrin (AGRN), N(G), N(G)-dimethylarginine dimethylaminohydrolase 1 (DDAH1), apolipoprotein E (APOE), syndecan-1 (SDC1), syndecan-2 (SDC2), glypican-2 (GPC2), apolipoprotein C-III (APOC3), apolipoprotein A-I (APOA1), syndecan-4 (SDC4), and glypican-6 (GPC6). The REACTOME network “sphingolipid de novo biosynthesis” contained eight identified proteins, namely aldehyde dehydrogenase family 3 member A2 (ALDH3A2), vesicle-associated membrane protein-associated protein A (VAPA), oxysterol-binding protein 1 (OSBP), serine palmitoyltransferase 1 (SPTLC1), sphingosine-1-phosphate lyase 1 (SGPL1), vesicle-associated membrane protein-associated protein B/C (VAPB), ceramide-transfer protein (CERT1), and 3-ketodihydrosphingosine reductase (KDSR). A Voronoi diagram representation of the pathway “metabolism” is shown in Figure 4.

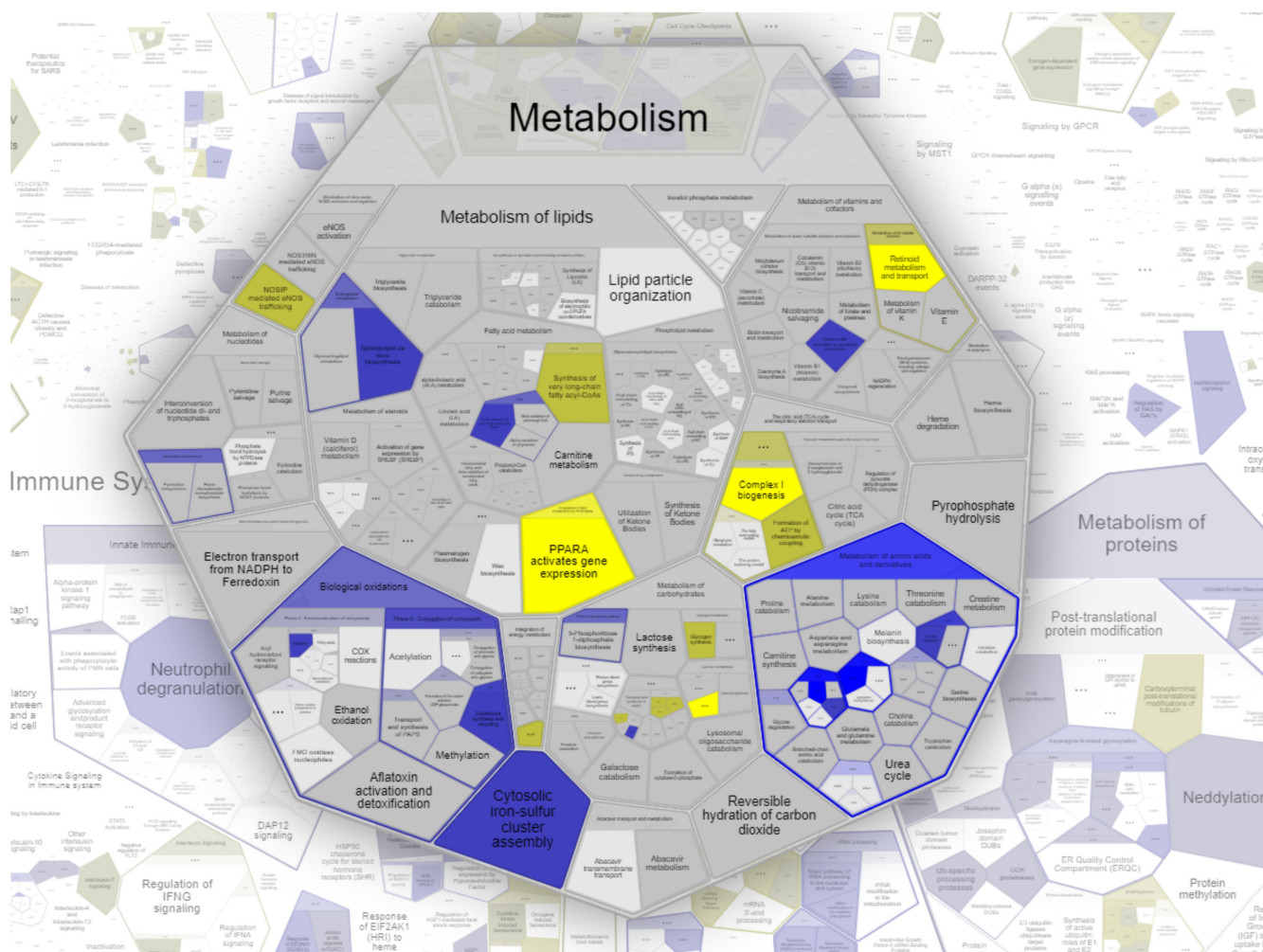


**Figure 4.** Voronoi diagram representation of the pathway “metabolism” by REACTOME analysis using all expressed protein elements of the WERI-RB1 and WERI-ETOR cell lines. Yellow colors show pathway activation in WERI-RB1 cells; blue colors show pathway activation in WERI-ETOR cells.

### 2.3. Drug-Enrichment Analysis of WERI-RB1 and WERI-ETOR Protein Signatures

To investigate if a certain drug-activity or drug-sensitivity signature matches our protein-expression data, a drug-connectivity analysis using the L1000 database was carried out. The most striking finding of these data was that the correlation between the etoposide-resistant cell line WERI-ETOR and the parental cell line WERI-RB1 revealed a very similar MOA for topoisomerase inhibitors, e.g., etoposide for the resistant cell line (Figure 5). These data demonstrate that topoisomerase inhibitors (most left) induce specific molecular changes, which are already active in WERI-ETOR cells. In turn, topoisomerase inhibitors lose their drug efficacy in these cell lines. ATPase inhibitors, acetylcholine receptor antagonists, and VEGFR inhibitors (most right) display the opposite MOA compared to WERI-ETOR cells and should thus overcome the developed therapy resistance.

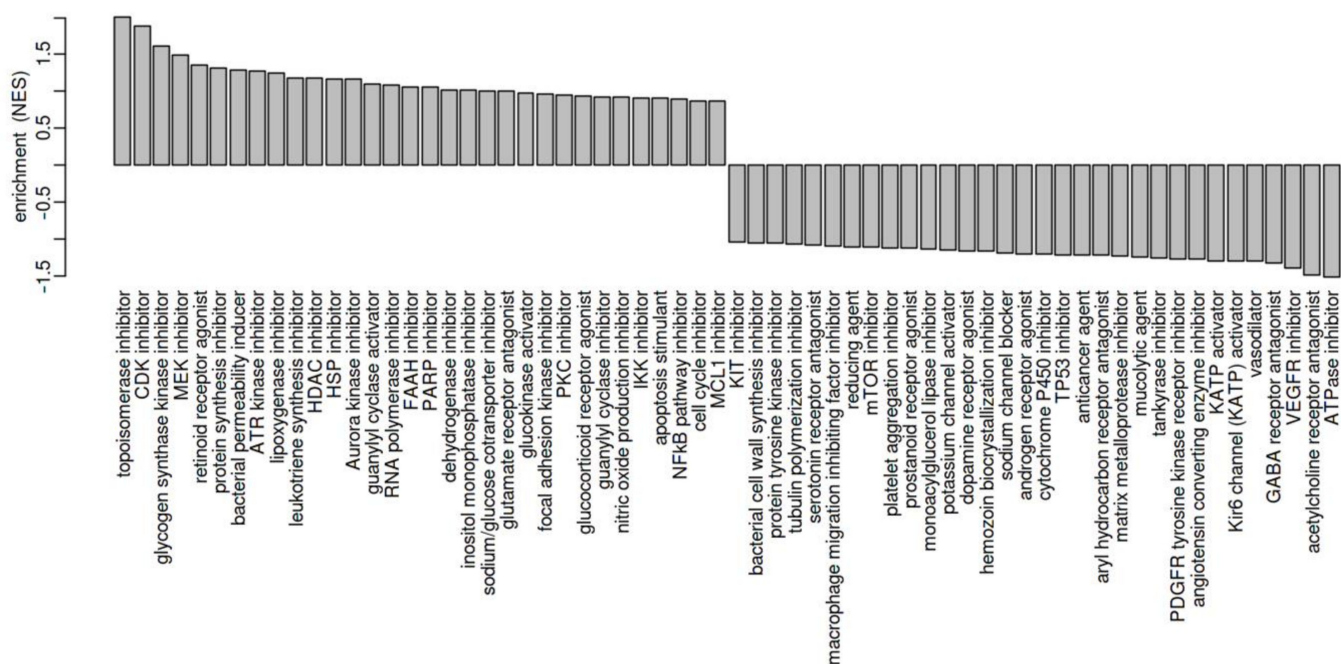


**Figure 5.** Visualization of the mechanism of action (MOA) across enriched drug profiles using the L1000 database. On the vertical axis, the GSEA normalized enrichment score of the MOA class is plotted.

### 3. Discussion

Drug resistance in RB is a clinical problem that can lead to the enucleation of a child's eye to prevent distant metastasis. The present study was designed to characterize the RB cell line WERI-RB1 and its etoposide-resistant subclone WERI-ETOR at the global proteome level. The comparison of both cell lines identified 64 differentially expressed proteins ( $\log_2FC$  of  $| > 2 |$  and a  $q$ -value  $< 0.05$ ; 22 higher and 42 lower expressed in WERI-ETOR). Pathway analysis by REACTOME algorithms revealed the most enriched metabolic pathway “retinoid metabolism and transport” for WERI-ETOR, while “sphingolipid de novo biosynthesis” was activated in WERI-RB1. These results support previous findings that linked RB samples with healthy biospecimens: Danda et al. identified a total of 3587 proteins using isobaric tags for relative and absolute quantitation (iTRAQ)-based quantitative mass spectrometric analysis and found 899 differentially expressed proteins between RB and healthy human retina samples [25]. Using the ingenuity pathway knowledge database, the top identified molecular and cellular processes were lipid metabolism, molecular transportation, small molecule biochemistry, nucleic acid metabolism as well as DNA replication, recombination, and repair [25]. Cheng et al., on the other hand, analyzed aqueous humor samples from RB patients and compared them with samples from patients without intraocular cancer using the comparative proteomic technique of iTRAQ coupled with offline two-dimensional liquid chromatography-tandem mass spectrometry. A total of 83 proteins were identified to be differentially expressed of which 44 were upregulated and 39 downregulated in the RB group [26]. Assisted by the DAVID bioinformatics resource, protein expression in RB has been implicated in endopeptidase inhibitory activity, peptidase inhibitor, enzyme inhibitor, serine-type endopeptidase inhibitor, structural molecule, lipid binding, and carbohydrate-binding activities [26]. Furthermore, in a different setting, Danda and colleagues performed proteomic analysis on human RB and healthy retina samples. A total of 3122 proteins were detected in this study, with 282 upregulated and 381 downregulated proteins in the RB sample [27]. Using the DAVID bioinformatics resource, the analysis revealed that most of the regulated proteins were primarily involved in glycoprotein, amyloid acute-inflammatory, and defensive responses. Furthermore, Naru et al. analyzed a human papilloma virus-positive RB sample, a human

papilloma virus-negative RB sample, and healthy human retina tissue [28]. Collectively, 2828 proteins were identified in this study. While 78 proteins were differentially expressed between the human papilloma virus-positive RB sample and the human healthy control retina sample, 88 proteins showed a differential expression between the human papilloma virus-negative RB sample and the human healthy control retina tissue. Bioinformatic analysis performed with the PANTHER classification system showed that most of these proteins were involved in catalytic activity, binding activity, structural molecule activity, enzyme regulator activity, transporter activity, receptor activity, antioxidant activity, nucleic acid binding transcription factor activity, and translation regulator activity [28]. Finally, Galardi et al. performed proteomic profiling by high-resolution MS of exosomes from a primary RB tumor cell line and a primary RB cell line established from vitreous seeds, which resulted in the identification of 3637 proteins [29]. Gene-enrichment analysis of exclusively and differentially expressed proteins and network analysis detected upregulated proteins related to invasion and metastasis involving extracellular matrix remodeling and interaction, resistance to anoikis, and the metabolism of glucose and amino acids in RB vitreous seeds exosomes [29]. Taken together, these proteomic analyses had in common that a more invasive or metastatic RB situation was associated with signaling pathways related to proliferation or inhibition of cell death as well as modulation of the ECM.

Complementary to the previous results, our study identified 4756 proteins by data-independent MS and revealed differences between the etoposide-sensitive WERI-RB1 and the etoposide-resistant WERI-ETOR cell lines. In accordance with other studies, proteins known to be associated with aggressiveness in other tumors, e.g., JAM2 (junctional adhesion molecule-A) [30], were found differentially expressed. Interestingly, pathway analysis revealed induction of, e.g., the “retinoid metabolism and transport” pathway in WERI-ETOR cells. This result is consistent with a study by Nicoud et al., which demonstrated that subretinal delivery of Y79 RB cell-infected retinoid-binding protein gene promoters led to the formation of photoreceptor cells in the mouse retina [31]. In line with this, Vene et al. showed that N-(4-hydroxyphenyl) retinamide inhibited RB tumor growth in a mouse model in vivo and induced cell death in Y79 RB cells in vitro [32]. Khanna et al. detected that retinoic acid upregulates neural retina leucine zipper, a transcription factor expressed in photoreceptors in Y79 [33]. In contrast, Kyritsis et al. have demonstrated an inhibitory effect of retinol and retinoic acid on the RB cell line Y79 [34].

Interestingly, as constituents of the “retinoid metabolism and transport” network, we also identified the heparan sulfate proteoglycans (HSPGs) and membrane-linked ECM receptors glypican-2 and -6 as well as syndecan-1, -2, and -4 downregulated in the WERI-ETOR cell line. As components of the tumor microenvironment, ECM proteins play a critical role in tumor growth and metastasis [35]. In this regard, we previously observed an extensive remodeling of various ECM components in the WERI-ETOR compared to the WERI-RB1 cell line, indicating that the ECM also plays a role in mediating chemotherapy-resistance formation of RB [15]. HSPGs are key players in various processes during neural development and malignant situations [35,36]. They preferentially bind to the basal lamina of blood vessels as well as to ependymal and endothelial surfaces, where they act as disposal sites for a variety of cytokines and growth factors [37]. Particularly, syndecan-1 and -2 have been described to influence VEGF-dependent neovascularization, which is an important mechanism to influence RB growth [38–40]. Lau et al. observed a reduced glypican-6 mRNA level in RB associated with non-random allelic loss at 13q31 that could contribute to the development of RB [41].

Furthermore, we observed an activation of the “sphingolipid de novo biosynthesis” pathway in WERI-RB1, which could most likely induce apoptosis and therefore, lead to an etoposide vulnerability. Several studies already noted the effect of sphingolipids on cancer [42]. A previous study by our group revealed a functional association between the sphingolipid metabolism and WERI-ETOR resistance, consistent with the results from our current proteomics study [14]. After exposure to etoposide, sphingosine, an apoptotic mediator, was upregulated in WERI-RB1 and WERI-ETOR, but only in WERI-ETOR, the

anti-apoptotic mediator sphingosine-1-phosphate was upregulated [14]. Additionally, Kim et al. noted that exposure to bisphenol A alters transcriptomic and proteomic dynamics in the RB cell line Y79 [43].

According to these data of pathway activation, we can infer that both “retinoid metabolism and transport” and “sphingolipid de novo biosynthesis” may play an important role during therapy resistance in RB. Our results are in line with these studies, which also observed the promotion of retinal cell genesis and may increase the resistance of the WERI-ETOR.

The most relevant finding in the clinical context was the similar MOA of topoisomerase inhibitors but the different MOA of ATPase inhibitors, acetylcholine receptor antagonists, and VEGFR inhibitors compared to WERI-ETOR. Hence, these findings suggest that biochemical processes of topoisomerase inhibitors as well as WERI-ETOR are likely to share the same “positive” molecules, including their expression data. It may, therefore, be the case that etoposide does not affect WERI-ETOR cell populations and, thus, induce no therapeutic activity. Furthermore, and for the same reasons, we speculate that ATPase inhibitors, acetylcholine receptor antagonists, and/or VEGFR inhibitors may be more effective treatment options for etoposide-resistant RB. To develop a complete picture of new treatment strategies in RB, additional studies will be needed that investigate WERI-ETOR and WERI-RB1 using drug classes, as suggested above.

Nevertheless, our study had some limitations. Our *in vitro* cell model only partially mimics chemotherapy resistance in RB *in vivo*. Therefore, to further test our hypothesis regarding the potential mechanism of resistance in RB, experiments in an animal model may be promising as a next step. Also, the pathway, as well as the MOA enrichment analysis, were only examined under untreated conditions for WERI-RB1 and WERI-ETOR. Along these lines, future experiments should investigate how both cell lines respond to recommended alternative treatment options.

## 4. Materials and Methods

### 4.1. Cell Culture

The RB cell lines, WERI-RB1 and WERI-ETOR, were cultivated, as previously described [13–17]. The identities of these RB cell lines were verified by DNA fingerprinting and profiling with eight different and highly polymorphic short tandem repeat (STR) loci (Leibniz-Institute DSMZ GmbH, Braunschweig, Germany). The generated STR profiles of the cell lines confirmed a full match of the respective parental reference STR profiles as determined by searching the following cell bank databases: ATCC (Manassas, VA, USA), JCRB (Osaka, Japan), RIKEN (Ibaraki, Japan), KCLB (Seoul, Korea), and DSMZ (Braunschweig, Germany). The purity of both cell lines was demonstrated by analysis of mitochondrial DNA sequences from mouse, rat as well as Chinese and Syrian hamster cells. Analyses with a detection limit of  $1:10^5$  showed the absence of mitochondrial sequences from foreign species.

### 4.2. Cell Preparation and Mass Spectrometry

Mass spectrometric analysis was performed, as described elsewhere [44]. Briefly, the Pierce<sup>TM</sup> Mass Spec Sample Prep Kit for Cultured Cells (Thermo Scientific, Waltham, MA, USA) was used for the preparation and precipitation of peptides according to the manufacturer’s instructions. Cell lysis buffer was used to first lyse  $10^6$  cells ( $n = 5/\text{group}$ ), and DNA and RNA were enzymatically digested using nuclease for cell lysis. Total protein concentration was subsequently determined using the fluorescence-based EZQ<sup>TM</sup> Protein Quantitation Kit (Life Technologies, Carlsbad, CA, USA) according to the manufacturer’s protocol. Briefly, protein samples were spotted, fixed onto an assay paper, and then stained with the proprietary fluorescence reagent. Fluorescence visualization was done with the Typhoon<sup>TM</sup> FLA 9000 laser scanner (GE Healthcare, Chicago, IL, USA). Subsequently, 50  $\mu\text{g}$  proteins were reduced, alkylated, and precipitated. Enzymatic protein digestion was then carried out by adding the digestion buffer and Lys-C protease to the acetone-precipitated

protein pellet. The samples were then frozen at  $-80^{\circ}\text{C}$  with trypsin storage solution to stop digestion.

The samples were lyophilized, resuspended in solvent A (0.1% FA) to a final concentration of  $1\ \mu\text{g}/\text{mL}$ , and were loaded into the HPLC (Thermo Scientific, Waltham, MA, USA). The reconstituted peptides were first desalted on a trap column (Luna,  $5\ \mu\text{m}$  C18 (2),  $20 \times 0.3\ \text{cm}$ ; Phenomenex, Torrance, CA, USA) and separated on an analytical column (LC Column,  $3\ \mu\text{m}$  C18 (2),  $150\ \text{mm} \times 0.3\ \text{mm}$ , Phenomenex, Torrance, CA, USA) using a multi-step gradient of solvent B (0.1% FA in ACN) in solvent A for 90 min at a flow rate of  $5\ \mu\text{L}/\text{min}$ . Mass spectra were acquired on a Triple ToF 5600+ (SciEX, Framingham, MA, USA) in a data-independent (SWATH) acquisition mode. The working parameters of the MS were ion spray voltage floating at 5000 V; ion source gas 1, 15; ion source gas 2, 0; curtain gas, 30; source temperature,  $0^{\circ}\text{C}$ . The optimized declustering potential (DP) was set at 100 V. The SWATH acquisition parameters were as follows: one 0.49965 s MS scan ( $m/z$  400–1250), followed by 100 variable Q1 windows with the size range 4.6–40.9 Da with 1 Da overlap.

#### 4.3. SWATH Data and Quantitative Data Processing

The raw SWATH files were processed using the software tool DIA-NN v1.7.16 (data-independent acquisition by neural networks) developed by Vadim Demichev et al. [24]. The “match between runs” function was used to first develop a spectral library from data-independent acquisition data. The precursor ion-generation settings were set to a peptide length of 7–52 amino acids, a maximum number of missed cleavages to one, and a maximum number of variable modifications to zero. The precursor and fragment ion  $m/z$  range were 350–1250  $m/z$ . A full analysis log, including the used processing settings, is included in Supplementary Table S3.

Precursors that passed the FDR cutoff of 0.01 were grouped into protein-/gene-groups. The protein groups were reduced to the first listed identifier for those groups consisting of multiple identifiers. The duplicates from a protein group resembling were removed.

The filtered dataset was further processed in the software tool Perseus [45]. MVs were imputed by random numbers drawn from a normal distribution with a width of 0.3 and a downshift of 1.8 (default settings) and total matrix imputation mode. The resulting data matrix was used for subsequent statistical analysis.

MS data have been deposited to the ProteomeXchange Consortium via the PRIDE partner repository [46] with the dataset identifier PXD030924.

#### 4.4. Data and Statistical Analysis

Protein data were partly analyzed with the software Omics Playground (BigOmics Analytics, v2.8.5 [47]). Cluster analyses were carried out using the t-distributed stochastic neighbor-embedding (tSNE) algorithm. To increase the statistical reliability of the protein-expression differences, we performed the analysis using commonly accepted methods in the literature, including Welch *t*-test, limma, edgeR as well as DESeq2, and merged the results (meta.*q* value corresponds to the highest *p*-value derived from the used methods). Significant differential protein expression was considered at a *q*-value of  $<0.05$  and a logarithmic fold-change ( $\log_2\text{FC}$ ) of  $|\geq 2|$ . Additionally, a variable importance score for each protein was calculated using multiple machine-learning algorithms, including LASSO [48], elastic nets [49], random forests [50], and extreme gradient boosting [51]. An aggregated score was computed and evaluated as the cumulative rank of the variable importance of the different algorithms. The top features were characterized by the highest cumulative ranks. The findings of the machine-learning algorithms were used to validate our marker panels derived from classical statistical tests.

#### 4.5. Pathway Enrichment and Drug-Connectivity Correlation

Pathway enrichment was performed using the REACTOME-pathway resource ([www.reactome.org](http://www.reactome.org), [52]) to understand high-level protein functions and to link information from

large molecular data sets. The REACTOME camera workflow, with a focus on metabolic pathways, was used to analyze the function of all quantitative data. Protein signatures were further correlated to known drug profiles from the L1000 database [53] by running the gene set enrichment analysis (GSEA) algorithm [54].

## 5. Conclusions

Our study identified over 4700 proteins in both cell lines examined and further discovered significant differences between WERI-RB1 and WERI-ETOR. In particular, the pathways “retinoid metabolism and transport” and “sphingolipid de novo biosynthesis” seem to play important roles in etoposide resistance, which could further clarify the understanding of resistance in RB. By drug-connectivity analysis using the L1000 database, this study also revealed a similar MOA for topoisomerase inhibitors and WERI-ETOR but a different MOA and potential new treatment options for ATPase inhibitors, acetylcholine receptor antagonists, and VEGFR inhibitors. Taken together, our study, which characterized WERI-RB1 and WERI-ETOR as a cell line model for the human situation in RB, offers new treatment ideas that should be tested in upcoming experiments. Additionally, validation of found differences in protein expression is warranted.

**Supplementary Materials:** The following supporting information can be downloaded at: <https://www.mdpi.com/article/10.3390/ijms23074058/s1>.

**Author Contributions:** Conceptualization, V.K. and J.R.; formal analysis, V.K., T.G., T.S. and J.R.; funding acquisition, V.K., M.M.K. and T.S.; methodology, V.K., T.G., M.M.K., S.C.J., S.M. and J.R.; writing—original draft, V.K., T.G., T.S. and J.R.; writing—review and editing, M.M.K., A.T., M.R., S.G., S.C.J. and S.M. All authors have read and agreed to the published version of the manuscript.

**Funding:** We are grateful for grant support (KinderAugenKrebsStiftung KAKS2019118f-UKL to V.K.). M.M.K. was gratefully supported by the Karl and Charlotte Spohn Stiftung. T.S. was gratefully supported by the Ad Infinitum Foundation.

**Institutional Review Board Statement:** Not applicable.

**Informed Consent Statement:** Not applicable.

**Data Availability Statement:** The mass spectrometry proteomics data have been deposited to the ProteomeXchange Consortium via the PRIDE partner repository [46] with the dataset identifier PXD030924.

**Acknowledgments:** We thank Andreas Faissner for his constant support. We also thank Sabine Kindermann and Sandra Lata for their technical assistance. We thank Jin Hee Choi for editing the manuscript for language and style purpose. This work was supported by Martin Eisenacher and his group from the Medizinisches Proteom-Center and Center for Protein Diagnostics—ProDi, German Network for Bioinformatics Infrastructure, service center BioInfra.Prot, funded by the German Federal Ministry of Education and Research (BMBF)—Grant FKZ 031 A 534A. This manuscript has been released as a preprint at bioRxiv [55].

**Conflicts of Interest:** The authors declare no conflict of interest. T.G. is a member of the BigOmics Analytics Advisory Board.

## References

1. Dimaras, H.; Corson, T.W.; Cobrinik, D.; White, A.; Zhao, J.; Munier, F.L.; Abramson, D.H.; Shields, C.L.; Chantada, G.L.; Njuguna, F.; et al. Retinoblastoma. *Nat. Rev. Dis. Primers* **2015**, *1*, 15021. [[CrossRef](#)] [[PubMed](#)]
2. Fabian, I.D.; Onadim, Z.; Karaa, E.; Duncan, C.; Chowdhury, T.; Scheimberg, I.; Ohnuma, S.I.; Reddy, M.A.; Sagoo, M.S. The management of retinoblastoma. *Oncogene* **2018**, *37*, 1551–1560. [[CrossRef](#)] [[PubMed](#)]
3. Kivela, T. The epidemiological challenge of the most frequent eye cancer: Retinoblastoma, an issue of birth and death. *Br. J. Ophthalmol.* **2009**, *93*, 1129–1131. [[CrossRef](#)] [[PubMed](#)]
4. Dimaras, H.; Kimani, K.; Dimba, E.A.; Gronsdahl, P.; White, A.; Chan, H.S.; Gallie, B.L. Retinoblastoma. *Lancet* **2012**, *379*, 1436–1446. [[CrossRef](#)]
5. Jain, M.; Rojanaporn, D.; Chawla, B.; Sundar, G.; Gopal, L.; Khetan, V. Retinoblastoma in Asia. *Eye* **2019**, *33*, 87–96. [[CrossRef](#)]

6. Houston, S.K.; Murray, T.G.; Wolfe, S.Q.; Fernandes, C.E. Current update on retinoblastoma. *Int. Ophthalmol. Clin.* **2011**, *51*, 77–91. [[CrossRef](#)]
7. Ward, E.; DeSantis, C.; Robbins, A.; Kohler, B.; Jemal, A. Childhood and adolescent cancer statistics, 2014. *CA Cancer J. Clin.* **2014**, *64*, 83–103. [[CrossRef](#)]
8. Sanders, B.M.; Draper, G.J.; Kingston, J.E. Retinoblastoma in Great Britain 1969–80: Incidence, treatment, and survival. *Br. J. Ophthalmol.* **1988**, *72*, 576–583. [[CrossRef](#)]
9. McFall, R.C.; Sery, T.W.; Makadon, M. Characterization of a new continuous cell line derived from a human retinoblastoma. *Cancer Res.* **1977**, *37*, 1003–1010.
10. McFall, R.C.; Nagy, R.M.; Nagle, B.T.; McGreevy, L.M. Scanning electron microscopic observation of two retinoblastoma cell lines. *Cancer Res.* **1978**, *38*, 2827–2835.
11. Busch, M.; Philippeit, C.; Weise, A.; Dunker, N. Re-characterization of established human retinoblastoma cell lines. *Histochem. Cell Biol.* **2015**, *143*, 325–338. [[CrossRef](#)]
12. Stephan, H.; Boeloeni, R.; Eggert, A.; Bornfeld, N.; Schueler, A. Photodynamic therapy in retinoblastoma: Effects of verteporfin on retinoblastoma cell lines. *Investig. Ophthalmol. Vis. Sci.* **2008**, *49*, 3158–3163. [[CrossRef](#)]
13. Mergler, S.; Cheng, Y.; Skosyrski, S.; Garreis, F.; Pietrzak, P.; Kociok, N.; Dwarakanath, A.; Reinach, P.S.; Kakkassery, V. Altered calcium regulation by thermosensitive transient receptor potential channels in etoposide-resistant WERI-Rb1 retinoblastoma cells. *Exp. Eye Res.* **2012**, *94*, 157–173. [[CrossRef](#)]
14. Kakkassery, V.; Skosyrski, S.; Luth, A.; Kleuser, B.; van der Giet, M.; Tate, R.; Reinhard, J.; Faissner, A.; Joachim, S.C.; Kociok, N. Etoposide Upregulates Survival Favoring Sphingosine-1-Phosphate in Etoposide-Resistant Retinoblastoma Cells. *Pathol. Oncol. Res.* **2019**, *25*, 391–399. [[CrossRef](#)]
15. Reinhard, J.; Wagner, N.; Kramer, M.M.; Jarocki, M.; Joachim, S.C.; Dick, H.B.; Faissner, A.; Kakkassery, V. Expression Changes and Impact of the Extracellular Matrix on Etoposide Resistant Human Retinoblastoma Cell Lines. *Int. J. Mol. Sci.* **2020**, *21*, 4322. [[CrossRef](#)]
16. Oronowicz, J.; Reinhard, J.; Reinach, P.S.; Ludwiczak, S.; Luo, H.; Omar Ba Salem, M.H.; Kraemer, M.M.; Biebermann, H.; Kakkassery, V.; Mergler, S. Ascorbate-induced oxidative stress mediates TRP channel activation and cytotoxicity in human etoposide-sensitive and -resistant retinoblastoma cells. *Lab. Invest.* **2021**, *101*, 70–88. [[CrossRef](#)]
17. Busch, M.; Papior, D.; Stephan, H.; Dunker, N. Characterization of etoposide- and cisplatin-chemoresistant retinoblastoma cell lines. *Oncol. Rep.* **2018**, *39*, 160–172. [[CrossRef](#)]
18. Zschoche, M.; Skosyrski, S.; Babst, N.; Ranjbar, M.; Rommel, F.; Kurz, M.; Tura, A.; Joachim, S.C.; Kociok, N.; Kakkassery, V. Islet Co-Expression of CD133 and ABCB5 in Human Retinoblastoma Specimens. *Klin. Monbl. Augenheilkd.* **2021**. Online ahead of print. [[CrossRef](#)]
19. Pane, K.; Affinito, O.; Zanfardino, M.; Castaldo, R.; Incoronato, M.; Salvatore, M.; Franzese, M. An Integrative Computational Approach Based on Expression Similarity Signatures to Identify Protein-Protein Interaction Networks in Female-Specific Cancers. *Front. Genet.* **2020**, *11*, 612521. [[CrossRef](#)]
20. Infante, T.; Franzese, M.; Ruocco, A.; Schiano, C.; Affinito, O.; Pane, K.; Memoli, D.; Rizzo, F.; Weisz, A.; Bontempo, P.; et al. ABCA1, TCF7, NFATC1, PRKCZ, and PDGFA DNA methylation as potential epigenetic-sensitive targets in acute coronary syndrome via network analysis. *Epigenetics* **2021**, 1–17. [[CrossRef](#)]
21. Chater-Diehl, E.; Goodman, S.J.; Cytrynbaum, C.; Turinsky, A.L.; Choufani, S.; Weksberg, R. Anatomy of DNA methylation signatures: Emerging insights and applications. *Am. J. Hum. Genet.* **2021**, *108*, 1359–1366. [[CrossRef](#)] [[PubMed](#)]
22. Van Eyk, J.E.; Snyder, M.P. Precision Medicine: Role of Proteomics in Changing Clinical Management and Care. *J. Proteome Res.* **2019**, *18*, 1–6. [[CrossRef](#)] [[PubMed](#)]
23. Jylha, A.; Nattinen, J.; Aapola, U.; Mikhailova, A.; Nykter, M.; Zhou, L.; Beuerman, R.; Uusitalo, H. Comparison of iTRAQ and SWATH in a clinical study with multiple time points. *Clin. Proteom.* **2018**, *15*, 24. [[CrossRef](#)] [[PubMed](#)]
24. Demichev, V.; Messner, C.B.; Vernardis, S.I.; Lilley, K.S.; Ralser, M. DIA-NN: Neural networks and interference correction enable deep proteome coverage in high throughput. *Nat. Methods* **2020**, *17*, 41–44. [[CrossRef](#)] [[PubMed](#)]
25. Danda, R.; Ganapathy, K.; Sathe, G.; Madugundu, A.K.; Ramachandran, S.; Krishnan, U.M.; Khetan, V.; Rishi, P.; Keshava Prasad, T.S.; Pandey, A.; et al. Proteomic profiling of retinoblastoma by high resolution mass spectrometry. *Clin. Proteom.* **2016**, *13*, 29. [[CrossRef](#)]
26. Cheng, Y.; Meng, Q.; Huang, L.; Shi, X.; Hou, J.; Li, X.; Liang, J. iTRAQ-based quantitative proteomic analysis and bioinformatics study of proteins in retinoblastoma. *Oncol. Lett.* **2017**, *14*, 8084–8091. [[CrossRef](#)]
27. Danda, R.; Ganapathy, K.; Sathe, G.; Madugundu, A.K.; Krishnan, U.M.; Khetan, V.; Rishi, P.; Gowda, H.; Pandey, A.; Subramanian, K.; et al. Membrane Proteome of Invasive Retinoblastoma: Differential Proteins and Biomarkers. *Proteom. Clin. Appl.* **2018**, *12*, e1700101. [[CrossRef](#)]
28. Naru, J.; Aggarwal, R.; Mohanty, A.K.; Singh, U.; Bansal, D.; Kakkar, N.; Agnihotri, N. Identification of differentially expressed proteins in retinoblastoma tumors using mass spectrometry-based comparative proteomic approach. *J. Proteom.* **2017**, *159*, 77–91. [[CrossRef](#)]
29. Galardi, A.; Colletti, M.; Lavarello, C.; Di Paolo, V.; Mascio, P.; Russo, I.; Cozza, R.; Romano, A.; Valente, P.; De Vito, R.; et al. Proteomic Profiling of Retinoblastoma-Derived Exosomes Reveals Potential Biomarkers of Vitreous Seeding. *Cancers* **2020**, *12*, 1555. [[CrossRef](#)]

30. Orlandella, F.M.; Mariniello, R.M.; Iervolino, P.L.C.; Auletta, L.; De Stefano, A.E.; Ugolini, C.; Greco, A.; Mirabelli, P.; Pane, K.; Franzese, M.; et al. Junctional adhesion molecule-A is down-regulated in anaplastic thyroid carcinomas and reduces cancer cell aggressiveness by modulating p53 and GSK3 alpha/beta pathways. *Mol. Carcinog.* **2019**, *58*, 1181–1193. [[CrossRef](#)]
31. Nicoud, M.; Kong, J.; Iqbal, S.; Kan, O.; Naylor, S.; Gouras, P.; Allikmets, R.; Binley, K. Development of photoreceptor-specific promoters and their utility to investigate EIAV lentiviral vector mediated gene transfer to photoreceptors. *J. Gene Med.* **2007**, *9*, 1015–1023. [[CrossRef](#)]
32. Vene, R.; Arena, G.; Poggi, A.; D'Arrigo, C.; Mormino, M.; Noonan, D.M.; Albin, A.; Tosetti, F. Novel cell death pathways induced by N-(4-hydroxyphenyl)retinamide: Therapeutic implications. *Mol. Cancer Ther.* **2007**, *6*, 286–298. [[CrossRef](#)]
33. Khanna, H.; Akimoto, M.; Siffroi-Fernandez, S.; Friedman, J.S.; Hicks, D.; Swaroop, A. Retinoic acid regulates the expression of photoreceptor transcription factor NRL. *J. Biol. Chem.* **2006**, *281*, 27327–27334. [[CrossRef](#)]
34. Kyritsis, A.; Joseph, G.; Chader, G.J. Effects of butyrate, retinol, and retinoic acid on human Y-79 retinoblastoma cells growing in monolayer cultures. *J. Natl. Cancer Inst.* **1984**, *73*, 649–654.
35. Theocharis, A.D.; Skandalis, S.S.; Tzanakakis, G.N.; Karamanos, N.K. Proteoglycans in health and disease: Novel roles for proteoglycans in malignancy and their pharmacological targeting. *FEBS J.* **2010**, *277*, 3904–3923. [[CrossRef](#)]
36. Faissner, A.; Reinhard, J. The extracellular matrix compartment of neural stem and glial progenitor cells. *Glia* **2015**, *63*, 1330–1349. [[CrossRef](#)]
37. Reinhard, J.; Brosicke, N.; Theocharidis, U.; Faissner, A. The extracellular matrix niche microenvironment of neural and cancer stem cells in the brain. *Int. J. Biochem. Cell Biol.* **2016**, *81*, 174–183. [[CrossRef](#)]
38. Corti, F.; Wang, Y.; Rhodes, J.M.; Atri, D.; Archer-Hartmann, S.; Zhang, J.; Zhuang, Z.W.; Chen, D.; Wang, T.; Wang, Z.; et al. N-terminal syndecan-2 domain selectively enhances 6-O heparan sulfate chains sulfation and promotes VEGFA165-dependent neovascularization. *Nat. Commun.* **2019**, *10*, 1562. [[CrossRef](#)]
39. Wang, L.; Chen, N.; Cheng, H. Fisetin inhibits vascular endothelial growth factor-induced angiogenesis in retinoblastoma cells. *Oncol. Lett.* **2020**, *20*, 1239–1244. [[CrossRef](#)]
40. Abu El-Asrar, A.M.; Nawaz, M.I.; De Hertogh, G.; Alam, K.; Siddiquei, M.M.; Van den Eynde, K.; Mousa, A.; Mohammad, G.; Geboes, K.; Opdenakker, G. S100A4 is upregulated in proliferative diabetic retinopathy and correlates with markers of angiogenesis and fibrogenesis. *Mol. Vis.* **2014**, *20*, 1209–1224.
41. Lau, C.S.; Yu, C.B.; Wong, H.K.; Fan, D.S.; Mak, H.T.; Wong, K.W.; Lam, D.S.; Pang, C.P.; Choy, K.W. Allelic imbalance at 13q31 is associated with reduced GPC6 in Chinese with sporadic retinoblastoma. *Br. J. Ophthalmol.* **2010**, *94*, 357–362. [[CrossRef](#)] [[PubMed](#)]
42. Hannun, Y.A.; Obeid, L.M. Principles of bioactive lipid signalling: Lessons from sphingolipids. *Nat. Rev. Mol. Cell Biol.* **2008**, *9*, 139–150. [[CrossRef](#)] [[PubMed](#)]
43. Kim, C.H.; Kim, M.J.; Park, J.; Kim, J.Y.; An, M.J.; Shin, G.S.; Lee, H.M.; Kim, J.W. Bisphenol A Exposure Changes the Transcriptomic and Proteomic Dynamics of Human Retinoblastoma Y79 Cells. *Genes* **2021**, *12*, 264. [[CrossRef](#)] [[PubMed](#)]
44. Sauer, T.; Facchinetti, G.; Kohl, M.; Kowal, J.M.; Rozanova, S.; Horn, J.; Schmal, H.; Kwee, I.; Schulz, A.P.; Hartwig, S.; et al. Protein Expression of AEBP1, MCM4, and FABP4 Differentiate Osteogenic, Adipogenic, and Mesenchymal Stromal Stem Cells. *Int. J. Mol. Sci.* **2022**, *23*, 2568. [[CrossRef](#)]
45. Tyanova, S.; Temu, T.; Sinitcyn, P.; Carlson, A.; Hein, M.Y.; Geiger, T.; Mann, M.; Cox, J. The Perseus computational platform for comprehensive analysis of (prote)omics data. *Nat. Methods* **2016**, *13*, 731–740. [[CrossRef](#)]
46. Perez-Riverol, Y.; Csordas, A.; Bai, J.; Bernal-Llinares, M.; Hewapathirana, S.; Kundu, D.J.; Inuganti, A.; Griss, J.; Mayer, G.; Eisenacher, M.; et al. The PRIDE database and related tools and resources in 2019: Improving support for quantification data. *Nucleic Acids Res.* **2019**, *47*, D442–D450. [[CrossRef](#)]
47. Akhmedov, M.; Martinelli, A.; Geiger, R.; Kwee, I. Omics Playground: A comprehensive self-service platform for visualization, analytics and exploration of Big Omics Data. *NAR Genom. Bioinform.* **2020**, *2*, lqz019. [[CrossRef](#)]
48. Friedman, J.; Hastie, T.; Tibshirani, R. Regularization Paths for Generalized Linear Models via Coordinate Descent. *J. Stat. Softw.* **2010**, *33*, 1–22. [[CrossRef](#)]
49. Zou, H.; Hastie, T. Regularization and variable selection via the elastic net. *J. R. Stat. Soc. Ser. B (Stat. Methodol.)* **2005**, *67*, 301–320. [[CrossRef](#)]
50. Breiman, L. Random Forests. *Mach. Learn.* **2001**, *45*, 5–32. [[CrossRef](#)]
51. Chen, T.; Guestrin, C. XGBoost: A Scalable Tree Boosting System. In Proceedings of the 22nd ACM SIGKDD International Conference on Knowledge Discovery and Data Mining, San Francisco, CA, USA, 13–17 August 2016; pp. 785–794.
52. Griss, J.; Viteri, G.; Sidiropoulos, K.; Nguyen, V.; Fabregat, A.; Hermjakob, H. ReactomeGSA—Efficient Multi-Omics Comparative Pathway Analysis. *Mol. Cell Proteom.* **2020**, *19*, 2115–2125. [[CrossRef](#)]
53. Subramanian, A.; Narayan, R.; Corsello, S.M.; Peck, D.D.; Natoli, T.E.; Lu, X.; Gould, J.; Davis, J.F.; Tubelli, A.A.; Asiedu, J.K.; et al. A Next Generation Connectivity Map: L1000 Platform and the First 1,000,000 Profiles. *Cell* **2017**, *171*, 1437–1452.e17. [[CrossRef](#)]
54. Subramanian, A.; Tamayo, P.; Mootha, V.K.; Mukherjee, S.; Ebert, B.L.; Gillette, M.A.; Paulovich, A.; Pomeroy, S.L.; Golub, T.R.; Lander, E.S.; et al. Gene set enrichment analysis: A knowledge-based approach for interpreting genome-wide expression profiles. *Proc. Natl. Acad. Sci. USA* **2005**, *102*, 15545–15550. [[CrossRef](#)]
55. Kakkassery, V.; Gemoll, T.; Krämer, M.M.; Sauer, T.; Tura, A.; Ranjbar, M.; Grisanti, S.; Joachim, S.C.; Mergler, S.; Reinhard, J. Protein profiling of WERI RB1 and etoposide resistant WERI ETOR reveals new insights into topoisomerase inhibitor resistance in retinoblastoma. *BioRxiv* **2022**, preprint. [[CrossRef](#)]